

A Bayesian Approach to Perceptual 3D Object-Part Decomposition using Skeleton-based Representations

Tarek El-Gaaly *

Department of Computer Science,
Rutgers University
Piscataway, NJ 08854, USA

Vicky Froyen †

Center for Cognitive Science,
Department of Psychology,
Rutgers University
Piscataway, NJ 08854, USA

Ahmed Elgammal

Department of Computer Science,
Rutgers University
Piscataway, NJ 08854, USA

Jacob Feldman and Manish Singh

Center for Cognitive Science,
Department of Psychology,
Rutgers University
Piscataway, NJ 08854, USA

Abstract

We present a probabilistic approach to shape decomposition that creates a skeleton-based shape representation of a 3D object while simultaneously decomposing it into constituent parts. Our approach probabilistically combines two prominent threads from the shape literature: skeleton-based (medial axis) representations of shape, and part-based representations of shape, in which shapes are combinations of primitive parts. Our approach recasts skeleton-based shape representation as a mixture estimation problem, allowing us to apply probabilistic estimation techniques to the problem of 3D shape decomposition, extending earlier work on the 2D case. The estimated 3D shape decompositions approximate human shape decomposition judgments. We present a tractable implementation of the framework, which begins by over-segmenting objects at concavities, and then probabilistically merges them to create a distribution over possible decompositions. This results in a hierarchy of decompositions at different structural scales, again closely matching known properties of human shape representation. The probabilistic estimation procedures that arise naturally in the model allow effective prediction of missing parts. We present results on shapes from a standard database illustrating the effectiveness of the approach.

Introduction

The goal of this work is to simultaneously decompose an object into its parts and compute a low-dimensional representation. For example, a coffee mug can be decomposed into the handle and the cylindrical vessel, and each of these primitive parts has a skeleton-based representation expressing its local symmetries (medial axes). The problem of interpreting 3D shape is fundamental in computer vision and robotics, especially with the increasing availability of 3D data.

In 1967, Blum published his pioneering work on representing 2D shapes using the Medial Axis Transform (MAT) (Blum 1967). The intuition behind MAT is that shapes are intuitively captured by a lower-dimensional representation

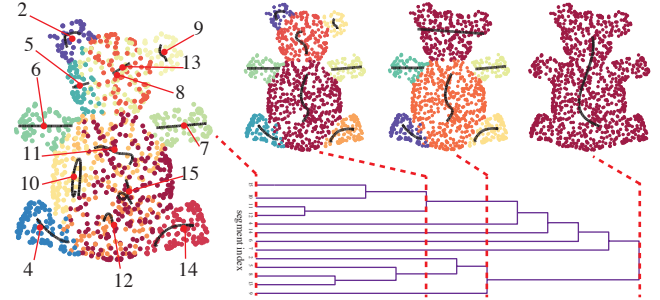


Figure 1: Dendrogram showing 3D decompositions of a 3D model point cloud. We show 4 decompositions in the hierarchy, starting (left) with an over-segmented interpretation and ending (right) with an under-segmented interpretation in which the whole object is represented as a single central axis. Each interpretation shows a segmentation (color-code) and the most probable skeletal axes under the model.

that extracts local symmetries of the shape's bounding contours, referred to as the medial axis. MAT computes the axis from the loci of centers of maximal discs contained within the shape. Evidence supporting medial representations can be found in psychophysics and neuroscience, with recent work showing neural representations in areas V4 and MT of the visual cortex (Hung, Carlson, and Connor 2012). On another front, early influential work has suggested that shapes can be recognized or classified based on their part decomposition (Marr and Nishihara 1978; Hoffman and Richards 1984; Biederman 1987). Both these lines of thought have led to enormous research literatures, but computational techniques for effectively decomposing 3D shapes into component parts remain poorly developed. These problems remain central challenges today, especially with the emergence of a plethora of 3D data and 3D sensor applications.

We present a *probabilistic* model of object-part decomposition and skeletonization of 3D objects. The contributions of this work are as follows. First, we present a probabilistic estimation procedure for 3D skeleton-based representations of point clouds. Second, simultaneously, our method decomposes an object into intuitively distinct parts. Third, our model allows us to assign degrees of belief (probabilis-

*Corresponding author: tgaaly@cs.rutgers.edu

†Corresponding author: vickyf@rutgers.edu

Copyright © 2015, Association for the Advancement of Artificial Intelligence (www.aaai.org). All rights reserved.

ties) to distinct part decomposition interpretations. Fourth, the model provides *hierarchical* interpretations, providing not just a single interpretation but a family of possible interpretations at different levels of abstraction, along with a probability distribution over them. This accords with characteristics of human perceptual organization, and moreover allows the computational system to interpret objects at multiple scales. Finally, the probabilistic nature of the model allows it to identify both the *most probable* object decomposition hypothesis and a distribution over a set of alternative hypotheses.

Related Work

Siddiqi and Pizer (2008) survey the many advances in shape representation since Blum. They divide shape understanding methods into several types, including landmark representations, boundary representations, displacement by voxel representations and medial representations. By far the most popular and intuitive shape representation is the medial representation. Numerous extension and improvements to the MAT have been proposed, including shock graphs (Macrini et al. 2002), reeb graphs (Biasotti et al. 2008), flux graphs (Rezanejad and Siddiqi 2013), object cores (Burbeck and Pizer 1995), multi-scale medial axes (Pizer et al. 1994), Bone graphs (Macrini et al. 2011), Bayesian estimation of the shape skeleton for 2D shapes (Feldman and Singh 2006; Froyen 2014). Problems with *ligatures*, noise, missing shape information due to occlusion and ambiguity in the final representation haunt many of these models because they inherit the basic limitations of Blum's approach (Rezanejad and Siddiqi 2013; Sebastian, Klein, and Kimia 2004). Improvements have been made by either smoothing over the object's shape before fitting the skeleton or smoothing the skeletal representation after fitting. A discussion of these methods appears in Miklos, Giesen, and Pauly (2010).

Most research on shape, including work nominally oriented towards the 2D case, takes the interpretation of 3D shape as the more fundamental problem (Hummel and Biederman 1992; Edelman 1997; Hummel and Stankiewicz 1998; Marr and Nishihara 1978; Feldman et al. 2013). Much of this work focuses on decomposition of shape into primitive parts that are not explicitly medial, and are applied to hand-crafted 3D objects rather than point-cloud data.

More recently, the Computer Graphics community has explored geometric methods for fitting skeletons to 3D shapes. The goal is to use these models to perform shape modelling and analysis for Computer Graphics applications. Two recent methods, Tagliasacchi, Zhang, and Cohen-Or (2009) and Huang et al. (2013), compute skeletons on incomplete and initially unorganized point clouds. The former computes a Rotational Symmetry Axis (ROSA) which captures local symmetry of the object shape. The latter approach improves upon this by creating an L1-median skeleton which locally adapts to the shape. There are many more previous approaches that fit skeletons to 3D object models, discussed further in Huang et al. (2013). Although these approaches are able to find 3D skeletons, they do so using a large set of free parameters, and are not able to assign graded beliefs to different possible decomposition interpretations.

One study (Ning et al. 2010) approaches the problem from a cognitive perspective by first decomposing objects into parts using segmentation and then computing critical/inflection points based on surface concavities. Skeletons are then extracted from segmented parts by joining them and refining the skeleton to represent the topology of the shape in accordance with *Morse Theory* (the basis for Reeb Graphs 1D skeletons and analyzing the topology of shapes using critical points). The emphasis in this approach on critical points and inflections reflects the prominent role they play in human shape representation (Winter and Wagemans 2006). However, in part because of its reliance on critical points, the method tends to fail in the presence of occlusion, though the human system can accommodate missing data with relative ease.

One approach that extracts 2D medial representations from 3D is Miklos, Giesen, and Pauly (2010). This approach, named the Discrete Scale Axis, improves upon Blum's original MAT for 3D objects by following the medial axis transform with topology-preserving angle filtering. Similarly, Siddiqi et al. (2008) proposed an algorithm for jointly computing the medial surfaces and object segmentations, resulting in a representation that yields favorable retrieval performance for rigid objects. The problem with 2D medial representations from a Computer Vision perspective (*i.e.* for object recognition/matching) is that 2D skeletal representation (*e.g.* sheets) is still relatively high dimensional. In Miklos, Giesen, and Pauly (2010) an example of this is the body of the dolphin which is represented by a relatively vertical sheet. This seems unnecessary for tubular shapes. A sufficient representation can be a curve going through the center of the dolphin's body with some definition of the cross-sectional variation along the main axis as in Biederman's definitions of 3D object parts (Biederman 1987). Despite this, some more rectangular objects require 2D representations, such as *sheets*.

Several approaches that focus on 3D mesh segmentation have achieved good performance on the Princeton Benchmark for 3D Mesh Segmentation (Chen, Golovinskiy, and Funkhouser 2009) and some also represent shapes using skeletons (Shapira, Shamir, and Cohen-Or 2008; Wong et al. 2014). Most of these approaches depend on the number segments/parts k being set prior to decomposition, except Core Extraction and Shape Diameter Function. The former decomposes an object hierarchically with a focus on pose invariance using feature points. No notion of probability is defined to identify more probable or intuitive decompositions and this method does not use skeletons to achieve the decomposition. The latter approach is similar to our approach. The authors jointly decompose objects and recover the skeleton using a probabilistic membership function (*i.e.* membership of a vertex into one of the object clusters/parts). The method performs well on articulated objects, but has trouble with non-articulated objects. Many of the aforementioned methods suffer from the same limitations as the traditional MAT approach, which stem from their inherently deterministic nature. Only a small number of approaches aim to estimate medial representations probabilistically. One example of this is Froyen (2014) who assumes

that the underlying skeleton is the generating source of the point-cloud. A probabilistic estimation procedure enables these approaches to handle noisy and missing information, assign beliefs to different decomposition interpretations, incorporate prior knowledge, and predict missing information. These approaches are, however, confined to 2D shapes, and probabilistic approaches have not yet been applied to the 3D case.

3D Perceptual Object-Part Decomposition

In this section we describe our 3D object-part decomposition approach. It is based on the idea that 3D object-part decomposition can be understood as a Bayesian mixture estimation problem. We propose a tractable implementation of this framework, which begins by over-segmenting objects at shape concavities, and then probabilistically merging them into a hierarchical representation, creating a distribution over possible decompositions.

Initial Over-Segmentation

The smallest unit of data we consider in this work is a segment of 3D points extracted by Over-Segmentation. In order to find these segments we use Normalized Cuts (Shi and Malik 2000), similar to Karpathy, Miller, and Fei-Fei (2013), that prefer segment cuts that lie along concavities. This mimics human perception as humans perceive part boundaries to be concave while the individual parts of the object tend to be convex (Hoffman and Richards 1984; Karpathy, Miller, and Fei-Fei 2013).

Our approach is set up such that Normalized Cuts computes the minimal cuts in the graph connecting the 3D points of the point cloud. The graph edges are assigned weights based on angles between neighboring points' surface normals as follows:

$$w_{ij} = \frac{e^{-\alpha(n_i \cdot (p_j - p_i))/2\sigma}}{d_{ij}} \quad (1)$$

where i is the subscript for the central point and j is for the neighbors of point p_i . n are the normals of the corresponding points and d_{ij} is the Euclidean distance between the points. When angles between n_i and $(p_j - p_i)$ are $> 90^\circ$, this means that the surface is convex. The weights in equation 1 are larger for more convex surfaces. Additionally, we penalize concavities by using a large α value when the angle is $< 90^\circ$ and using a small α for convex angles $> 90^\circ$. This ensures that optimal cuts are along surface concavities.

The segments found in this way, shown in Fig. 2, serve as the basic building blocks in our hierarchical approach below and in addition we use the normalized cut values as an additional cue in determining most-probable merges in the hierarchy. The normalized cut values are equal to the normalized sum of weights on edges of optimal cuts. We scale these optimal cuts in the 0-1 range and combine them with the posterior probabilities of merging two segments. This is described further in the Hierarchical Grouping section.

Generative 3D Skeletal Representation

Our approach is based on a framework found in Froyen (2014) for perceptual grouping in general, and 2D part-



Figure 2: Over-Segmentation results for arbitrary large k values. Notice concavities on the surface of the objects constitute good cut boundaries.

decomposition specifically, called Bayesian Hierarchical Grouping (BHG). This framework has been shown to make qualitative and quantitative predictions of human behavior across several areas of perceptual grouping, including 2D part-decomposition. Here we apply the framework to the realm of 3D object decomposition with some novel extensions.

Mixture Model Within BHG each possible part decomposition interpretation $c_j \in \mathbf{C} = \{\mathbf{c}_1 \dots \mathbf{c}_J\}$ of a set of 3D points $D = \{x_1 \dots x_N\}$ is associated with a posterior probability $p(\mathbf{C}|D)$, which according to Bayes rule is proportional to the product of a prior probability $p(\mathbf{C})$ and a likelihood $p(D|\mathbf{C})$. Here a decomposition hypothesis \mathbf{c}_j is a vector of labels $\mathbf{c}_j = \{c_1 \dots c_N\}$ assigning each set of 3D points x_n to a part m . By adopting the BHG framework, both the 3D part decomposition problem and 3D skeletonization can be viewed as a mixture estimation problem. We assume that the configuration of 3D points making up a 3D shape is generated by a mixture of M underlying skeletal axes:

$$p(x_n|\phi) = \sum_{m=1}^M p(x_n|\theta_m)p(c_n = m|\mathbf{p}) \quad (2)$$

where $c_n \in \mathbf{c} = \{c_1 \dots c_N\}$ are the assignments of data to an axis, \mathbf{p} is a parameter vector of a multinomial distribution with $p(c_n = m|\mathbf{p}) = p_m$, θ_m are the parameters of the m -th axis, and $\phi = \{\theta_1, \dots, \theta_M, \mathbf{p}\}$. Since the problem of estimating mixture consists of estimating which axis m owns which point x_n and the parameters θ of the underlying axes, both the decomposition problem and the 3D skeletonization problem are solved in tandem.

Generative Function The generative function $p(x_n|\theta_m)$ depicting how 3D points are generated from an underlying axis generalizes the skeletal generating function proposed in Feldman and Singh (2006) and Froyen (2014). A flexible way of representing (and encoding) axes is by means of a 3D parametric B-spline curve $g_m(t)$ (Fig. 3), governed by a parameter vector \mathbf{q}_m . From this curve data points are generated from a univariate Gaussian distribution perpendicular to the curve,

$$p(x_n|\theta_m) = \mathcal{N}(d_n|a_m t_n + b_m, \sigma_m)$$

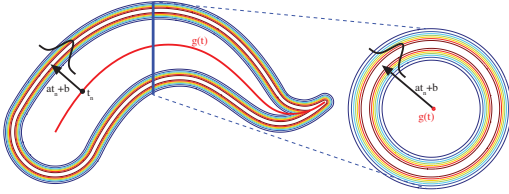


Figure 3: Two cuts showing our 3D generative function. Red line depicts the underlying B-spline axis. The gradient depicts the probability $p(x_n|\theta)$, where red has a higher probability.

where $d_n = ||x_n - g_m(n)||$, called the *riblength*, is the distance between the datapoint x_n and its perpendicular projection on the curve $g_m(n)$, referred to as the *footpoint*. The mean of the normal distribution is defined as a linear function of the footpoint positions t_n , with slope a_m , intercept b_m and σ_m is variance over the riblengths (Fig. 3). Together parameter vector for the generative function becomes $\theta_m = \{a_m, b_m, \sigma_m, q_m\}$. Note that the generative function constrains parts to obey a kind of local symmetry, and the linear function over riblengths allows us to capture conic parts.

In keeping with a full-fledged Bayesian approach a set of priors over the generative function's parameters θ_m is defined, summarized by $p(\theta|\beta)$. Two priors are introduced over the curve g_m itself: one over the squared arclength F_{1m} of the curve g_m , $F_{1m} \sim \exp(\lambda_1)$ and one over the squared total curvature F_{2m} of the curve g_m , $F_{2m} \sim \exp(\lambda_2)$, both respectively governing the elastic and bending energy of the curve. Lastly, a conjugate prior to the normal distribution is adopted. The prior over the variance σ is $\sigma \sim \mathcal{X}^{-\epsilon}(\sigma_0, \nu_0)$, where σ_0 depicts the mean variance of the riblength, and ν_0 how strongly we believe this. The slope a and intercept b both have a Gaussian prior distribution, $a \sim \mathcal{N}(\mu_0, \kappa_0^{-1})$ and $b \sim \mathcal{N}(\mu_0, \kappa_0^{-1})$. Thus the hyperparameter vector is defined as $\beta = \{\mu_0, \kappa_0, \sigma_0, \nu_0, \lambda_1, \lambda_2\}$

In order to compute the likelihood of a particular decomposition hypothesis $p(D|\mathbf{c}_j)$, it is important to integrate over the axis parameters θ for each axis, resulting in the marginal likelihood $p(D_m|\beta) = \int p(D_m|\theta)p(\theta|\beta)d\theta$, where D_m are all the points x_n belonging to axis $c_n = m$. Unfortunately integrating over all possible curves (*i.e.* the parameter space of q_m) is computationally expensive. The marginal is approximated by only integrating over the Gaussian components, which due to the conjugate formulation can be done analytically, and selecting q_m as to maximize,

$$p(D_m|\beta, \mathbf{q}) = \int \prod_{c_n=m} p(x_n|a, b, \sigma)p(\theta|\beta)dadbd\sigma. \quad (3)$$

This equation is maximized as a function of \mathbf{q} , by means of a 2-step algorithm (for details see Flöry, 2005). In step 1 the footpoints t_n for each point x_n is computed. Given these pairs $[x_n, t_n]$, in step 2, we maximize the above equation using *Simulated Annealing* (Kirkpatrick, Gelatt, and Vecchi 1983). Both steps are then repeated until convergence. In this way we not only find an at least locally optimal skeletal axis

representation for a point cloud segment, but also (as incorporated in $p(D_m|\theta)$) we capture how "part-like" the segment is, given our prior assumptions.

Our approach should be formulated to be independent of any user-specified M components. To ensure independence, a Dirichlet process prior is used, as in Froyen (2014), over the decomposition hypotheses $p(\mathbf{c}_j|\alpha)$. In this way the above mixture model becomes a Dirichlet process mixture model which is a widely used non-parametric approach (Neal 2000). This results in the following definition of the above introduced posterior for a decomposition hypothesis:

$$p(\mathbf{c}_j|D, \alpha, \beta) \propto p(\mathbf{c}_j|\alpha) \prod_{m=1}^M p(D_m|\beta), \quad (4)$$

where M now denotes the number of axis specific to \mathbf{c}_j , and $p(\mathbf{c}_j|\alpha) = \int p(\mathbf{c}_j|\mathbf{p})p(\mathbf{p}|\alpha)d\mathbf{p}$ is a standard Dirichlet integral. Unfortunately the size of the hypothesis space \mathbf{C} is exponential in the number of 3D points, N . The BHG framework approximates this large posterior, by implementing a version of the Bayesian Hierarchical Clustering algorithm by Heller and Ghahramani (2005). Moreover, this approach results in an intuitive hierarchical representation of the configuration of 3D points.

Hierarchical Grouping

Bayesian hierarchical clustering (Heller and Ghahramani 2005) follows the same concept as traditional Agglomerative clustering algorithms, with the main difference that a Bayesian hypothesis test is used to decide which clusters to merge. Here we will briefly sketch the algorithm; for more details we refer to Heller and Ghahramani (2005). In our implementation the algorithm will initiate with K trees T_k each containing the set of 3D points D_k belonging to the k -th initial segment as found by the over-segmentation stage (see above and Fig. 1). At each iteration the algorithm decides which pair of trees (T_i and T_j) are most likely to be merged using a Bayesian hypothesis test, resulting in a new tree $T_{i \cup j}$ containing the data $D_{i \cup j} = D_i \cup D_j$. The pairs of segment regions of the point cloud are considered for merging if they are adjacent to each other in Euclidean space. This is a simple way of drastically reducing the complexity of the computation, since not all pairs must be considered.

In order to compute the likelihood of a merge, two hypothesis are compared. The first hypothesis \mathcal{H}_{merge} , treats all data $D_{i \cup j}$ as generated from one underlying axis, and can thus readily be computed as $p(D_{i \cup j}|\mathcal{H}_{merge}) = p(D_{i \cup j}|\beta)$ (see Eq. 3). We also benefit from information from the over-segmentation phase which is in the form of the cut values between neighboring segments. We take the product $\log p(D_{i \cup j}|\beta) = Cut(D_i, D_j) \log p(D_{i \cup j}|\beta)$ as our new marginal likelihood (adding to Eq. 3). This affects the probability of merging by preferring merges with high cut-values (*i.e.* less concavity between the segments).

The second hypothesis $\mathcal{H}_{nomerge}$, treats all data $D_{i \cup j}$ as generated by more than one axis as constrained by the tree structure. Its probability is computed by taking the product over the subtrees $p(D_{i \cup j}|\mathcal{H}_{nomerge}) = p(D_i|T_i)p(D_j|T_j)$.

Here $p(D_i|D_j)$ is computed recursively as the tree is built:

$$p(D_{i \cup j}|T_{i \cup j}) = p(\mathcal{H}_{\text{merge}})p(D_{i \cup j}|\mathcal{H}_{\text{merge}}) + (1 - p(\mathcal{H}_{\text{merge}}))p(D_i|T_i)p(D_j|T_j)$$

where $p(\mathcal{H}_{\text{merge}})$ is based on the Dirichlet process prior and is also computed recursively as the tree is built. The probability of a pair D_i and D_j being merged is:

$$r_{i \cup j} = \frac{p(D_{i \cup j}|\mathcal{H}_{\text{merge}})p(\mathcal{H}_{\text{merge}})}{p(D_{i \cup j}|T_{i \cup j})}$$

The pair with the highest probability of the merge hypothesis is then merged. In this way the algorithm continues to greedily build the tree until all data is merged into one tree. Note that each level along the tree depicts a different decomposition hypothesis (see Fig. 1). The probability of each of these hypotheses is easily computed using Eq. 4.

Experimental Discussion

We experimented on the 3D Dataset from Chen, Golovinskiy, and Funkhouser (2009), which provides a large dataset of 3D meshes - 380 objects across 19 different categories. We subsample the 3D meshes and reduce the representation to unorganized 3D point clouds. Each point has its corresponding computed surface normal which is used in over-segmentation. We uniformly subsample the point clouds, substantially reducing the number of points.

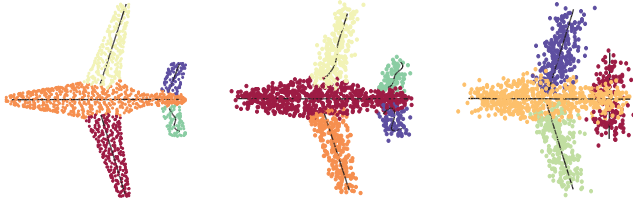


Figure 4: Added zero-mean Gaussian noise to one of the airplane object models. Despite noise of up 20% of the mean inter-point distance, the skeletonization and decomposition works well.

Figure 1 shows the hierarchical decomposition of a Teddy Bear. The two center decompositions shown correspond to local maxima of the posterior probability in the hierarchy. We find these to be among the most intuitive decompositions. Our maximum-a-posterior (MAP) decomposition is the second one from the right and corresponds exactly to 14 human annotated teddy bears. This particular object may be considered an “easy” example but more complex objects can be seen in Fig. 7 and some of their corresponding human segmented counterparts in Fig. 8.

We show that our object representations are somewhat robust to noise as shown in Fig. 4. We added Gaussian noise with zero-mean and standard deviation equal to 10-20% of the mean inter-point distance of neighboring points. As the noise increases we still obtain a relatively intuitive decomposition.

To validate the generative capability of our model on 3D data, we show how it performs in reverse by generating the

input data. Fig. 5 and Fig. 6 show the original subsampled input point cloud with sampled points from our underlying generative model overlaid. Figure 6 is particularly interesting. We remove a hole in the surface of the Martini Glass model and are able to reconstruct it by filling it up with points sampled from the Gaussian distribution of our underlying generative model.

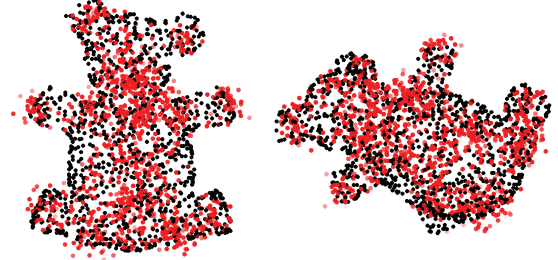


Figure 5: Black points are the subsampled input point cloud which is used to estimate the underlying generative model. Red points show sampled points from our underlying probabilistic model (the more opaque being more probable - best viewed using zoom).

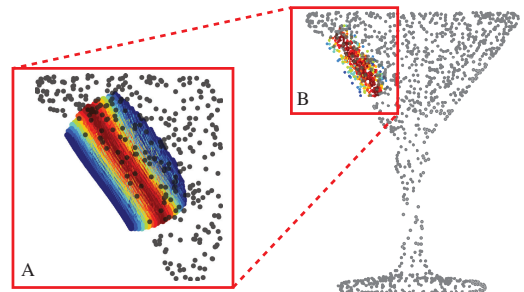


Figure 6: This figure shows the ability to predict missing data. Here a hole is cut into the side of object and it is filled by sampling from the underlying generative model. The heat map depicts the probability of that sample (with red being higher probability).

Conclusion

We have presented a novel procedure for estimating skeletal representations from 3D point clouds and decomposing them into intuitive component parts. We produce an intuitive hierarchical tree of abstractions and a distribution over them. These multiple representations of an object closely match known properties of human shape representation. We validate this by an experimental study as well as the capability of dealing with noise and predicting missing data which can occur due to occlusion.

Acknowledgments

The research was supported by NSF 1218872 and 1409683 to AE, and NIH EY021494 to JF and MS. The authors would like to thank Brian McMahan for motivating and helpful discussions.

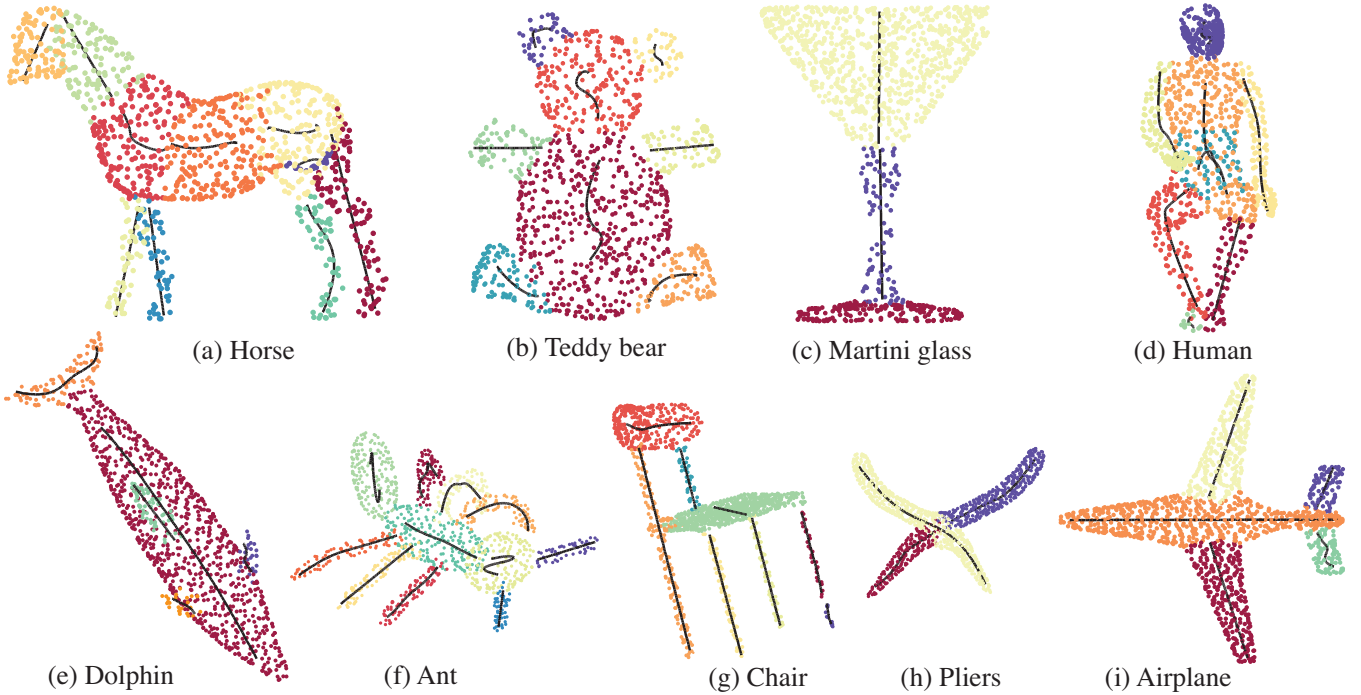


Figure 7: MAP object-part decomposition for a broad selection of 3D object models. The black curves in each colored segmented represents the estimated skeletal axis of that segment. Notice, for example, the ability to discriminate the 3 parts of the Martini glass. Notice also the ability to decompose both articulated and non-articulated objects. Some failure cases can be seen in (d). One or two problematic merges happen due to the non-symmetric torso. Despite this, the skeleton is not compromised.

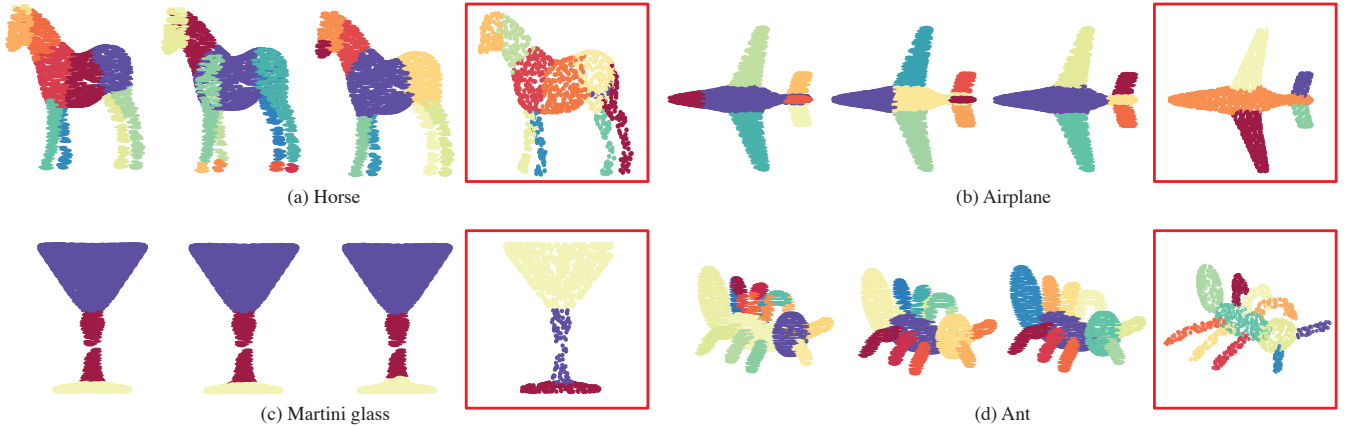


Figure 8: For comparison, these are a selection of 4 manually human segmented objects. Each object in the dataset has annotations corresponding to, on average, 11 human subject segmentations. MAP decompositions computed by our approach are shown in the red squares.

References

- [1] Biasotti, S.; Giorgi, D.; Spagnuolo, M.; and Falcidieno, B. 2008. Reeb graphs for shape analysis and applications. *Theoretical Computer Science* 392(1):5–22.
- [2] Biederman, I. 1987. Recognition-by-components: A theory of human image understanding. *Psychological Review* 94(2):115–147.
- [3] Blum, H. 1967. A transformation for extracting new descriptors of shape. In *Models for the Perception of Speech and Visual Form*.
- [4] Burbeck, C. A., and Pizer, S. M. 1995. Object representation by cores: Identifying and representing primitive spatial regions. *Vision Research* 35(13):1917–1930.
- [5] Chen, X.; Golovinskiy, A.; and Funkhouser, T. 2009. A benchmark for 3D mesh segmentation. In *SIGGRAPH*.
- [6] Edelman, S. 1997. Computational theories of object recognition. *Trends in Cognitive Science* 8(1):296–304.
- [7] Feldman, J., and Singh, M. 2006. Bayesian estimation of the shape skeleton. *Proceedings of the National Academy of Sciences* 103(47):18014–18019.
- [8] Feldman, J.; Singh, M.; Briscoe, E.; Froyen, V.; Kim, S.; and Wilder, J. 2013. An integrated bayesian approach to shape representation and perceptual organization. In Dickinson, S., and Pizlo, Z., eds., *Shape perception in human and computer vision*, Advances in Computer vision and pattern recognition. Springer.
- [9] Flöry, S. 2005. Fitting B-spline curves to point clouds in the presence of obstacles. Master’s thesis, TU Wien.
- [10] Froyen, V. 2014. *Bayesian Mixture Estimation For Perceptual Grouping*. Ph.D. Dissertation, Rutgers, The State University of New Jersey.
- [11] Heller, K., and Ghahramani, Z. 2005. Bayesian hierarchical clustering. In *ICML*.
- [12] Hoffman, D. D., and Richards, W. A. 1984. Parts of recognition. *Cognition* 18(1):65–96.
- [13] Huang, H.; Wu, S.; Cohen-Or, D.; Gong, M.; Zhang, H.; Li, G.; and B.Chen. 2013. L1-medial skeleton of point cloud. In *SIGGRAPH*.
- [14] Hummel, J. E., and Biederman, I. 1992. Dynamic binding in a neural network for shape recognition. *Psychological Review* 99(3):480–517.
- [15] Hummel, J. E., and Stankiewicz, B. J. 1998. Two roles for attention in shape perception: A structural description model of visual scrutiny. *Visual Cognition* 5:49–79.
- [16] Hung, C.-C.; Carlson, E. T.; and Connor, C. E. 2012. Medial axis shape coding in macaque inferotemporal cortex. *Neuron* 74(6):1099–1113.
- [17] Karpathy, A.; Miller, S.; and Fei-Fei, L. 2013. Object discovery in 3d scenes via shape analysis. In *ICRA*.
- [18] Kirkpatrick, S.; Gelatt, C. D.; and Vecchi, M. P. 1983. Optimization by simulated annealing. *Science* 220(4598):671–680.
- [19] Macrini, D.; Shokoufandeh, A.; Dickinson, S. J.; Siddiqi, K.; and Zucker, S. W. 2002. View-based 3-d object recognition using shock graphs. In *ICPR*.
- [20] Macrini, D.; Dickinson, S. J.; Fleet, D. J.; and Siddiqi, K. 2011. Bone graphs: Medial shape parsing and abstraction. *Computer Vision and Image Understanding* 115(7):1044–1061.
- [21] Marr, D., and Nishihara, H. K. 1978. Representation and recognition of the spatial organization of three-dimensional shapes. *Proceedings of the Royal Society of London* 200(1140):269–294.
- [22] Miklos, B.; Giesen, J.; and Pauly, M. 2010. Discrete scale axis representations for 3d geometry. In *SIGGRAPH*.
- [23] Neal, R. M. 2000. Markov chain sampling methods for dirichlet process mixture models. *Journal of computational and graphical statistics* 9(2):249–265.
- [24] Ning, X.; Li, E.; Zhang, X.; and Wang, Y. 2010. Shape decomposition and understanding of point cloud objects based on perceptual information. In *SIGGRAPH*.
- [25] Pizer, S. M.; Burbeck, C. A.; Coggins, J. M.; Fritsch, D. S.; and Morse, B. S. 1994. Object shape before boundary shape: Scale-space medial axes. *Journal of Mathematical Imaging and Vision* 4(3):303–313.
- [26] Rezanejad, M., and Siddiqi, K. 2013. Flux graphs for 2D shape analysis. In Dickinson, S., and Pizlo, Z., eds., *Shape perception in human and computer vision*, Advances in Computer vision and pattern recognition. Springer.
- [27] Sebastian, T. B.; Klein, P. N.; and Kimia, B. B. 2004. Recognition of shapes by editing their shock graphs. In *PAMI*.
- [28] Shapira, L.; Shamir, A.; and Cohen-Or, D. 2008. Consistent mesh partitioning and skeletonisation using the shape diameter function. *Visual Computation* 24(4):249–259.
- [29] Shi, J., and Malik, J. 2000. Normalized cuts and image segmentation. In *PAMI*.
- [30] Siddiqi, K., and Pizer, S. 2008. *Medial Representations: Mathematics, Algorithms and Applications*. Springer Publishing Company, Incorporated.
- [31] Siddiqi, K.; Zhang, J.; Macrini, D.; Shokoufandeh, A.; Bouix, S.; and Dickinson, S. 2008. Retrieving articulated 3-d models using medial surfaces. *Machine vision and applications* 19(4):261–275.
- [32] Tagliasacchi, A.; Zhang, H.; and Cohen-Or, D. 2009. Curve skeleton extraction from incomplete point cloud. In *SIGGRAPH*.
- [33] Winter, J. D., and Wagemans, J. 2006. Segmentation of object outlines into parts: A large-scale integrative study. *Cognition* 99(3):275–325.
- [34] Wong, S.-K.; Yang, J.-A.; Ho, T.-C.; and Chuang, J.-H. 2014. A skeleton-based approach for consistent segmentation transfer. *Journal of information science and engineering* 30(4):1053–1070.